

9. Fourier Optics

The Fourier transform plays an important role in science and technology. The one-dimensional Fourier transform \mathcal{F} , for instance, connects a time signal $f(t)$ with its complex spectral function $A(\nu)$ which gives information about the frequency content of the signal:

$$A(\nu) = \mathcal{F}[f(t)](\nu) = \int_{-\infty}^{+\infty} f(t) \exp(-2\pi i \nu t) dt. \quad (9.1)$$

In optics, mainly the two-dimensional Fourier transform applies. For instance, the electric field in the back focal plane of a convex lens is the two-dimensional spatial Fourier transform of the electric field $E(x,y)$ in the front focal plane of the lens. Similarly to (9.1), the two-dimensional Fourier transform $\tilde{E}(\nu_x, \nu_y)$ is defined by

$$\begin{aligned} \tilde{E}(\nu_x, \nu_y) &= \mathcal{F}[E(x,y)](\nu_x, \nu_y) \\ &= \int_{-\infty}^{+\infty} \int_{-\infty}^{+\infty} E(x,y) \exp[-2\pi i(\nu_x x + \nu_y y)] dx dy. \end{aligned} \quad (9.2)$$

Here, with a view to the frequency ν , the quantities ν_x and ν_y are called spatial frequencies. The basic definitions and relations pertaining to the Fourier transform are summarized in the Appendix. To understand why the Fourier transform occurs in many optical arrangements, we consider the diffraction of light at an aperture in the (x,y) -plane in the approximation of scalar diffraction theory.

9.1 Scalar Diffraction Theory

We consider the diffraction at a transparency having the transmittance distribution $\tau(x,y)$ in the plane $z = 0$. When illuminating it with a plane, linearly polarized monofrequency wave of wavelength λ , we obtain a wave field propagating into the half space behind, which we set out to describe (see Fig. 9.1).

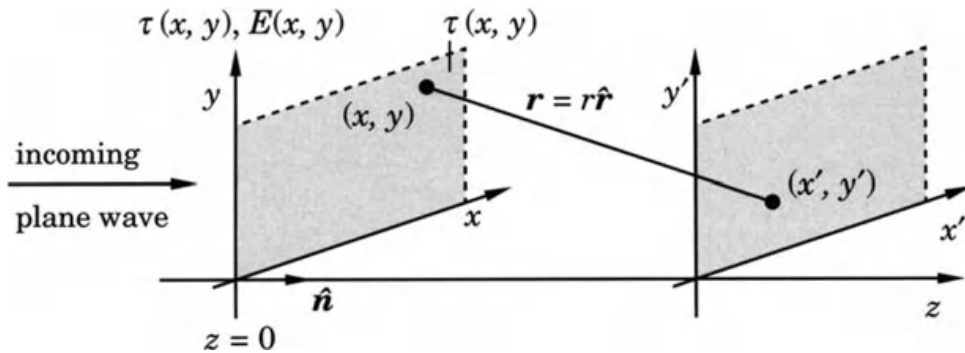


Fig. 9.1. Geometry for describing the diffraction of a plane wave at a transmittance distribution $\tau(x,y)$ in the plane where $z = 0$.

To begin, immediately behind the plane where $z = 0$ the field

$$E(x,y) = \tau(x,y)E_e(x,y) \quad (9.3)$$

is present, where $E_e(x,y)$ is the electric field strength of the incident wave in the $(x,y,0)$ -plane. To a good approximation, further propagation can be described by the assumption that each point $(x,y,0)$ of the diffraction pattern is the source of a spherical wave (Huygens' principle).

Then, in a plane with coordinates (x',y',z) (see Fig. 9.1), a field $E(x',y',z)$ is obtained given by the Kirchhoff diffraction integral:

$$E(x',y',z) = \frac{1}{i\lambda} \int_{-\infty}^{+\infty} \int_{-\infty}^{+\infty} E(x,y) \frac{1}{r} \exp(ikr) \cos(\hat{n}\hat{r}) dx dy. \quad (9.4)$$

Mainly, it corresponds to a sum of the spherical waves originating at all points $(x,y,0)$. Here, $1/i\lambda$ is a phase and amplitude factor and $\cos(\hat{n}\hat{r})$ is a directional factor. Both follow from Maxwell's equations, from which (9.4) is derived.

9.1.1 Fresnel Approximation

The Kirchhoff integral (9.4) is usually unwieldy and further approximations are needed for an analytical treatment. In the paraxial approximation, the coordinates of x and y and also x' and y' are restricted to values which are small compared to the distance z between the diffracting object and its diffraction pattern, that is, $|x|, |y| \ll z$ and $|x'|, |y'| \ll z$. This means that only rays which form a small angle with the optical axis, the z -axis, are considered. Then, to a good approximation, the cosine factor in the integrand can be neglected. Thus we can set

$$\cos(\hat{n}\hat{r}) = 1, \quad (9.5)$$

since all light rays travel almost parallel to the z -axis. Furthermore, the r -dependence of the amplitudes can be ignored. That is, since $r \approx z$, we

can set $1/r = 1/z$. However, this approximation is too coarse for the exponential function, because small changes in r lead to large changes in the phase kr . Here, the approximation is carried one step further. The square root in

$$r = \sqrt{(x' - x)^2 + (y' - y)^2 + z^2} = z \sqrt{1 + \frac{(x' - x)^2}{z^2} + \frac{(y' - y)^2}{z^2}} \quad (9.6)$$

is expanded into a power series and truncated after the second term:

$$r \approx z + \frac{(x' - x)^2}{2z} + \frac{(y' - y)^2}{2z}. \quad (9.7)$$

With these approximations, the Fresnel approximation to the diffraction integral is obtained:

$$E(x', y', z) = \frac{\exp(ikz)}{i\lambda z} \int_{-\infty}^{+\infty} \int_{-\infty}^{+\infty} E(x, y) \exp\left(\frac{ik}{2z} [(x' - x)^2 + (y' - y)^2]\right) dx dy. \quad (9.8)$$

This form of the diffraction integral lends itself to a different interpretation in the language of one-dimensional system theory. To this end, we define the function

$$h_z(x, y) = \frac{\exp(ikz)}{i\lambda z} \exp\left[i \frac{k}{2z} (x^2 + y^2)\right], \quad (9.9)$$

the impulse response of free space. Then, the Kirchhoff diffraction integral can be written as a convolution of the complex electric field distribution in the diffracting plane with the impulse response of free space:

$$E(x', y', z) = E(x, y) * h_z(x, y). \quad (9.10)$$

(Concerning the notion of convolution see the Appendix.) Indeed, from the definition of the convolution it is easily seen that the expression (9.10) is the Kirchhoff diffraction integral in the Fresnel approximation:

$$\begin{aligned} E(x', y', z) &= E(x, y) * h_z(x, y) \\ &= \int_{-\infty}^{+\infty} \int_{-\infty}^{+\infty} E(x, y) h_z(x' - x, y' - y) dx dy \\ &= \frac{\exp(ikz)}{i\lambda z} \int_{-\infty}^{+\infty} \int_{-\infty}^{+\infty} E(x, y) \exp\left(\frac{ik}{2z} [(x' - x)^2 + (y' - y)^2]\right) dx dy. \end{aligned} \quad (9.11)$$

The Fresnel approximation can also be written differently with the help of the Fourier transform. To this end, the expressions $(x' - x)^2$ and $(y' - y)^2$ are expanded and suitably collected:

$$E(x',y',z) = \frac{\exp(ikz)}{i\lambda z} \exp \left[i \frac{\pi}{\lambda z} (x'^2 + y'^2) \right] \\ \cdot \int_{-\infty}^{+\infty} \int_{-\infty}^{+\infty} E(x,y) \exp \left[i \frac{\pi}{\lambda z} (x^2 + y^2) \right] \exp \left[-2\pi i \left(\frac{x'}{\lambda z} x + \frac{y'}{\lambda z} y \right) \right] dx dy. \quad (9.12)$$

With the abbreviation

$$A(x',y',z) = \frac{\exp(ikz)}{i\lambda z} \exp \left[i \frac{\pi}{\lambda z} (x'^2 + y'^2) \right] \quad (9.13)$$

and the definition (9.2) of the Fourier transform, we can write

$$E(x',y',z) = A(x',y',z) \mathcal{F}[E(x,y) \exp(i\pi/\lambda z (x^2 + y^2))] \left(\frac{x'}{\lambda z}, \frac{y'}{\lambda z} \right). \quad (9.14)$$

Thus, the electric field in a plane where $z = \text{const}$ is given by a Fourier transform of the electric field distribution in the diffracting plane after multiplication with a quadratic phase factor $\exp[(i\pi/\lambda z)(x^2 + y^2)]$.

The Fresnel approximation yields good results for quite short distances from the diffracting plane, in many cases down to ten wavelengths only.

9.1.2 Fraunhofer Approximation

For large distances from the diffracting plane (far field) and for a finite size of the diffracting pattern in x and y , the quadratic phase term becomes small and may be neglected. More precisely, it is required that

$$z \gg \frac{\pi}{\lambda} (x^2 + y^2). \quad (9.15)$$

Then the quadratic phase factor becomes

$$\exp \left[i \frac{\pi}{\lambda z} (x^2 + y^2) \right] \approx 1, \quad (9.16)$$

corresponding to negligible curvature of the wave fronts, and the Fraunhofer approximation is obtained:

$$E(x',y',z) = A(x',y',z) \int_{-\infty}^{+\infty} \int_{-\infty}^{+\infty} E(x,y) \exp \left[-2\pi i \left(\frac{x'}{\lambda z} x + \frac{y'}{\lambda z} y \right) \right] dx dy. \quad (9.17)$$

If we introduce new coordinates

$$\nu_x = \frac{x'}{\lambda z} \quad \text{and} \quad \nu_y = \frac{y'}{\lambda z}, \quad (9.18)$$

the expression for the electric field reads

$$E(x',y',z) = A(\lambda z \nu_x, \lambda z \nu_y, z) \mathcal{F}[E(x,y)](\nu_x, \nu_y) = \tilde{E}(\nu_x, \nu_y). \quad (9.19)$$

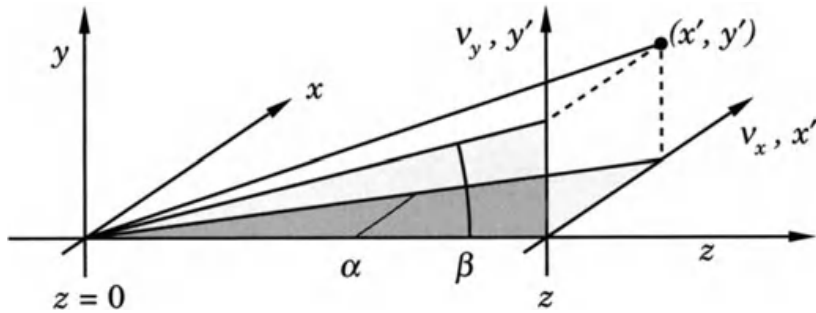


Fig. 9.2. Geometry for the definition of spatial frequencies.

The determination of the diffraction pattern in the far field has been reduced to a Fourier transform of the electric field distribution immediately behind the diffracting structure. The coordinates v_x and v_y introduced in (9.18) are called spatial frequencies. They are proportional to the corresponding diffraction angles α and β in the (x,z) - and the (y,z) -planes, respectively.

From Fig. 9.2 we find:

$$\begin{aligned} v_x &= \frac{x'}{\lambda z} = \frac{\tan \alpha}{\lambda} \approx \frac{\alpha}{\lambda}, \\ v_y &= \frac{y'}{\lambda z} = \frac{\tan \beta}{\lambda} \approx \frac{\beta}{\lambda}. \end{aligned} \quad (9.20)$$

The far-field or Fraunhofer approximation can be given a very intuitive interpretation. It is a decomposition of the light field $E(x,y)$ into plane waves propagating at angles α and β . As the approximation is valid for small α and β , we have $\tan \alpha \approx \sin \alpha \approx \alpha$ and $\tan \beta \approx \sin \beta \approx \beta$. Then the quantities x'/z and y'/z can be written as

$$\frac{x'}{z} \approx \sin \alpha \quad \text{and} \quad \frac{y'}{z} \approx \sin \beta. \quad (9.21)$$

This means that the exponential function in the integral of (9.17), along with the factor $\exp(ikz)$, represents a plane wave,

$$\exp(ikx \sin \alpha + iky \sin \beta + ikz), \quad (9.22)$$

that forms the angles α and β with the z -axis in the (x,z) - and (y,z) -planes, respectively. For given λ and z we have

$$v_x \propto \alpha \propto x', \quad v_y \propto \beta \propto y'. \quad (9.23)$$

Thus, the rays arriving at the far-field point (x', y') leave the (x,y) -plane at the angles $\alpha \propto x'$ and $\beta \propto y'$. Large angles correspond to high spatial frequencies, small angles to low spatial frequencies.

The diffraction pattern at the point (x',y',z) on a screen is given by the intensity $I = |E(x',y',z)|^2$. Because the modulus has to be taken, the phase factor

$$A = \exp(ikz) \exp\left[\frac{i\pi}{\lambda z} (x'^2 + y'^2)\right] \quad (9.24)$$

drops out, and the diffraction pattern is given, up to a factor, by the spatial power spectrum of the input field:

$$I(v_x, v_y) = \frac{1}{\lambda^2 z^2} |\mathcal{F}[E(x,y)](v_x, v_y)|^2. \quad (9.25)$$

From this relation we see that the diffraction pattern gets fainter the farther it is taken from the diffracting object and the larger the wavelength. Both facts are intuitively comprehended. At large wavelengths the light is diffracted more strongly and thus, per given solid angle, less light is available. At a larger distance z , the light in a given solid angle is distributed over a larger area in the (x',y') -plane.

9.2 Fourier Transform by a Lens

A convex lens of focal length f_l focuses parallel rays (plane waves) into the back focal plane (Fig. 9.3). The coordinate v of the focal point in the back focal plane, the (u,v) -plane, corresponds to the angle β the rays form in the (y,z) -plane or (v,z) -plane with the optical axis:

$$\frac{v}{f_l} = \tan \beta \approx \beta. \quad (9.26)$$

A corresponding relation holds for the coordinate u and the angle α . This means that the lens projects the far-field diffraction pattern into its back

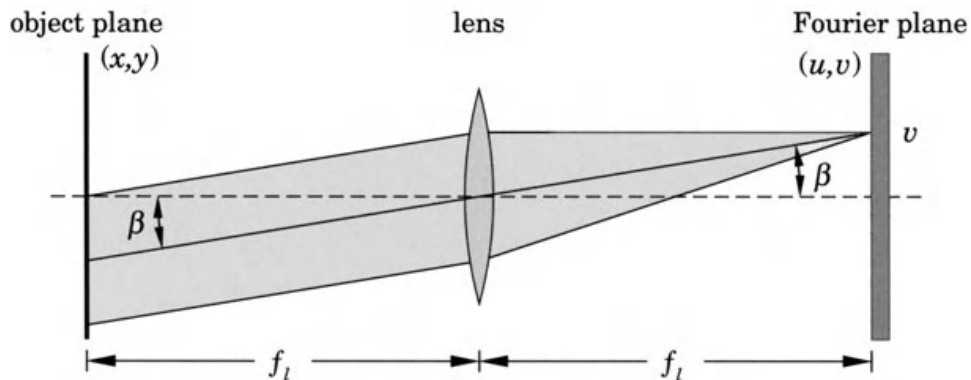


Fig. 9.3. Geometric configuration of rays for demonstrating the Fourier transform properties of a lens, $2f$ arrangement.

focal plane, since

$$\begin{aligned} v_x &= \frac{x'}{\lambda z} = \frac{\alpha}{\lambda} = \frac{u}{\lambda f_l}, \\ v_y &= \frac{y'}{\lambda z} = \frac{\beta}{\lambda} = \frac{v}{\lambda f_l}. \end{aligned} \quad (9.27)$$

Written in the coordinates $u = \lambda f_l v_x$ and $v = \lambda f_l v_y$ of the back focal plane, we have

$$\tilde{E}(u, v) = A(u, v, f_l) \int_{-\infty}^{+\infty} \int_{-\infty}^{+\infty} E(x, y) \exp \left[-2\pi i \left(\frac{u}{\lambda f_l} x + \frac{v}{\lambda f_l} y \right) \right] dx dy. \quad (9.28)$$

When the input field $E(x, y)$ is located in the front focal plane of the lens, the phase factor in A becomes independent of u and v . In this case the lens exactly performs a two-dimensional Fourier transform from the front to the back focal plane:

$$\tilde{E}(u, v) \propto \mathcal{F}[E(x, y)](u, v). \quad (9.29)$$

The function $\mathcal{F}[E(x, y)]$ is called the (complex) amplitude spectrum. Viewing or recording this spectrum again yields the power spectrum of $E(x, y)$:

$$I(u, v) = |\tilde{E}(u, v)|^2 \propto |\mathcal{F}[E(x, y)]|^2. \quad (9.30)$$

It is the diffraction pattern of the input and is simply called the spectrum. When the square of the modulus is taken, the phase factor drops out. Therefore the transparency can be placed anywhere in front of the lens for to obtain the diffraction pattern. To avoid vignetting effects the transparency is best placed directly in front of the lens (Fig. 9.4).

Often the diffraction pattern is very small. From the relationships $u = \lambda f_l v_x$ and $v = \lambda f_l v_y$ it follows that the diffraction pattern in the (u, v) -plane becomes larger the larger the focal length of the lens used. For the same reasons the ring system at the exit of a Fabry–Perot interferometer is projected with the help of a lens with a long focal length (e. g., $f_l = 1$ m).

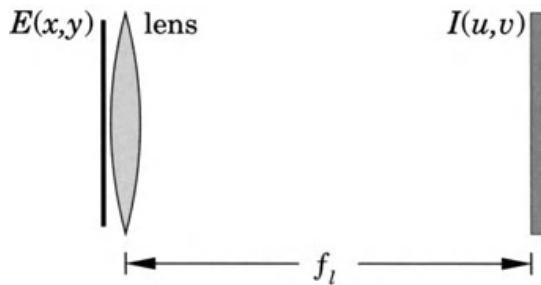


Fig. 9.4. Preferable geometry for obtaining the diffraction pattern.

9.3 Optical Fourier Spectra

In the following, we consider a few simple examples of the optical Fourier transform and illustrate them with a lens in the $2f$ geometry. Once the correspondence between the object distribution (input transparency) and its Fourier transform is understood in the examples, the main structures of the diffraction patterns of more complex objects can often be guessed by intuition and experience.

9.3.1 Point Source

A point source located at (x_0, y_0) in the plane $z = 0$ can be described by a two-dimensional Dirac δ function. We write it formally as a product of two one-dimensional δ functions:

$$E(x, y) = E_0 \delta(x - x_0) \delta(y - y_0). \quad (9.31)$$

Then a formal integration yields:

$$\begin{aligned} \mathcal{F}[E(x, y)] &= \int_{-\infty}^{+\infty} \int_{-\infty}^{+\infty} E_0 \delta(x - x_0) \delta(y - y_0) \exp[-2\pi i(\nu_x x + \nu_y y)] dx dy \\ &= E_0 \exp[-2\pi i(\nu_x x_0 + \nu_y y_0)]. \end{aligned} \quad (9.32)$$

Thus, the Fourier transform of a point source corresponds to the field of a plane wave. It appears in the back focal plane of a lens in a $2f$ geometry (Fig. 9.5). When the point source is located on the optical axis, that is, when $(x_0, y_0) = (0, 0)$, the plane wave propagates along the optical axis. For a point off the optical axis, $(x_0, y_0) \neq (0, 0)$, the wave propagates at an angle to the optical axis with $\alpha \approx x_0/f_l$ and $\beta \approx y_0/f_l$. In both cases, the power spectrum is constant, $|\mathcal{F}[E(x, y)]|^2 = |E_0|^2$; the back focal plane is illuminated uniformly.

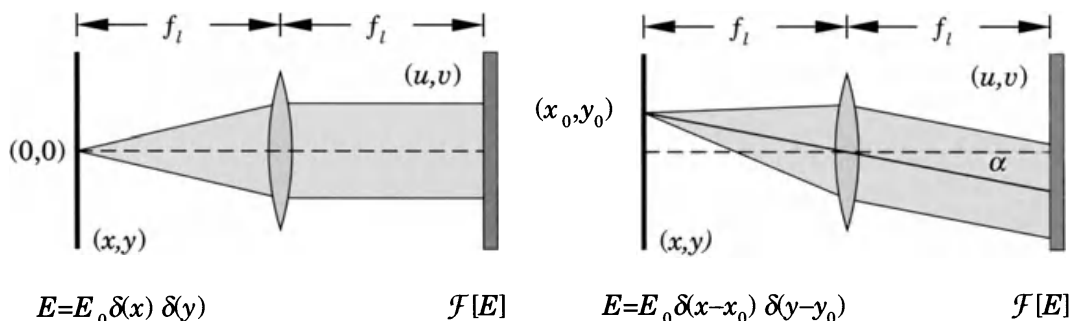


Fig. 9.5. Spectrum of a point source on the optical axis (left) and off axis (right).

9.3.2 Plane Wave

A plane wave propagating in the direction of the optical axis is of constant amplitude in the plane $z = 0$. Therefore the Fourier transform is given, up to a factor, by a two-dimensional δ function:

$$E(x,y) = E_0, \quad (9.33)$$

$$\begin{aligned} \mathcal{F}[E(x,y)] &= \int_{-\infty}^{+\infty} \int_{-\infty}^{+\infty} E_0 \exp[-2\pi i(\nu_x x + \nu_y y)] dx dy \\ &= E_0 \delta(\nu_x) \delta(\nu_y). \end{aligned} \quad (9.34)$$

Thus, a point appears at $(\nu_x, \nu_y) = (0,0)$ corresponding to $(u,v) = (0,0)$ in the back focal plane. The situation is depicted in Fig. 9.6.

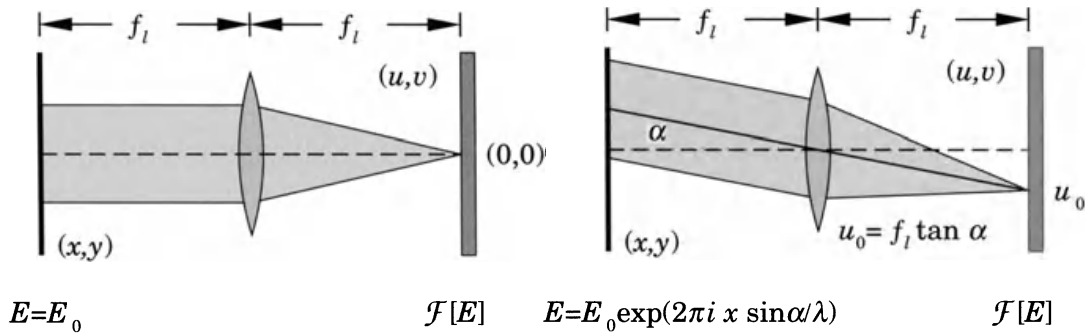


Fig. 9.6. Spectrum of a plane wave propagating along the optical axis (left) and at an angle α (right).

The electric field of a plane wave propagating obliquely to the optical axis at the angles α and β contains a space-dependent phase factor in the object plane $z = 0$. In the spectrum this leads to a shift of the focus point:

$$E(x,y) = E_0 \exp\left[\frac{2\pi i}{\lambda}(x \sin \alpha + y \sin \beta)\right], \quad (9.35)$$

$$\begin{aligned} \mathcal{F}[E(x,y)] &= \int_{-\infty}^{+\infty} \int_{-\infty}^{+\infty} E_0 \exp\left[\frac{2\pi i}{\lambda}(x \sin \alpha + y \sin \beta)\right] \exp[-2\pi i(\nu_x x + \nu_y y)] dx dy \\ &= E_0 \int_{-\infty}^{+\infty} \exp\left[-2\pi i\left(\nu_x - \frac{\sin \alpha}{\lambda}\right)x\right] dx \int_{-\infty}^{+\infty} \exp\left[-2\pi i\left(\nu_y - \frac{\sin \beta}{\lambda}\right)y\right] dy \\ &= E_0 \delta\left(\nu_x - \frac{\sin \alpha}{\lambda}\right) \delta\left(\nu_y - \frac{\sin \beta}{\lambda}\right). \end{aligned} \quad (9.36)$$

Again, the resulting spectrum is a single point, but at the spatial frequency $(\nu_x, \nu_y) = (\sin \alpha / \lambda, \sin \beta / \lambda)$. This corresponds, in the back focal plane, to a focus point at $u_0 = f_l \sin \alpha \approx \alpha f_l$ and $v_0 = f_l \sin \beta = \beta f_l$ (Fig. 9.6).

9.3.3 Infinitely Long Slit

Slits are often found as aperture stops in optical devices such as in spectrographs. To begin, we consider an infinitely narrow, infinitely long slit. We assume an illumination of the slit by a plane monofrequency wave of normal incidence; that is, the slit acts as a coherent line source:

$$E(x,y) = E_0 \delta(x), \quad (9.37)$$

$$\begin{aligned} \mathcal{F}[E(x,y)] &= E_0 \int_{-\infty}^{+\infty} \int_{-\infty}^{+\infty} \delta(x) \exp[-2\pi i(\nu_x x + \nu_y y)] dx dy \\ &= E_0 \int_{-\infty}^{+\infty} \exp(-2\pi i \nu_y y) dy = E_0 \delta(\nu_y). \end{aligned} \quad (9.38)$$

The Fourier transform thus yields another line, rotated by 90° with respect to the slit (Fig. 9.7).

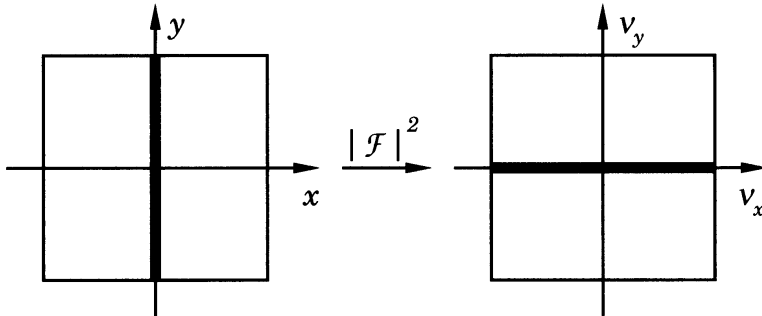


Fig. 9.7. Infinitely long, infinitely narrow slit and its spectrum.

An infinitely long slit of finite width a , illuminated as before, has an electric field given by the rect function:

$$E(x,y) = E_0 \text{rect}\left(\frac{x}{a}\right) = E_0 \times \begin{cases} 1 & \text{for } |x| < a/2, \\ 0 & \text{else,} \end{cases} \quad (9.39)$$

$$\begin{aligned} \mathcal{F}[E(x,y)] &= E_0 \int_{-\infty}^{+\infty} \int_{-a/2}^{+a/2} \exp[-2\pi i(\nu_x x + \nu_y y)] dx dy \\ &= E_0 \int_{-\infty}^{+\infty} \exp(-2\pi i \nu_y y) dy \int_{-a/2}^{+a/2} \exp(-2\pi i \nu_x x) dx \\ &= E_0 \delta(\nu_y) \frac{1}{-2\pi i \nu_x} [\exp(-2\pi i \nu_x a/2) - \exp(2\pi i \nu_x a/2)] \\ &= E_0 \delta(\nu_y) \frac{\sin(\pi \nu_x a)}{\pi \nu_x} = E_0 a \delta(\nu_y) \text{sinc}(a \nu_x). \end{aligned} \quad (9.40)$$

The sinc function just introduced is defined by

$$\text{sinc}(x) = \frac{\sin \pi x}{\pi x}. \quad (9.41)$$

Again, the spectrum has (practically) no extension in the v_y -direction. In the v_x -direction, the intensity is modulated with the square of the sinc function, the slit function (Fig. 9.8).

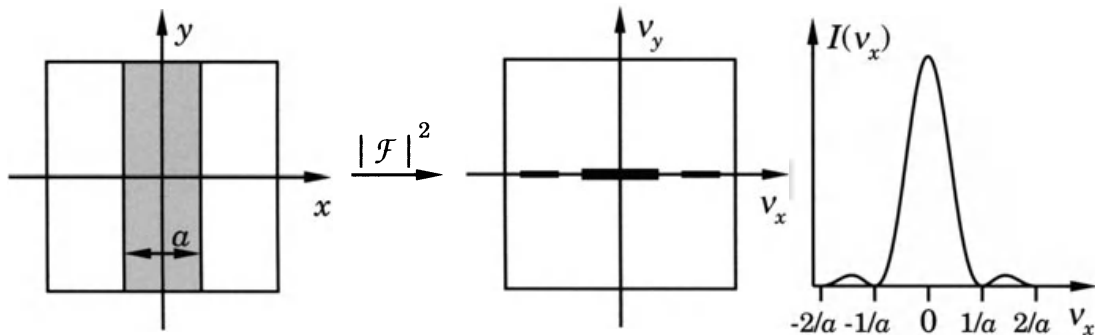


Fig. 9.8. Infinitely long slit of finite width and its power spectrum.

Figure 9.9 shows two experimentally obtained spectra of a long slit of different width a . When we use a variable slit whose width can be altered by turning a micrometer screw, the widening of the central maximum of the spectrum with decreasing slit width can be followed live. The broader the slit (that is, the larger a), the more closely spaced are the maxima in the spectrum. The roots of the sinc function are found at $\dots -2/a, -1/a, 1/a, 2/a \dots$.

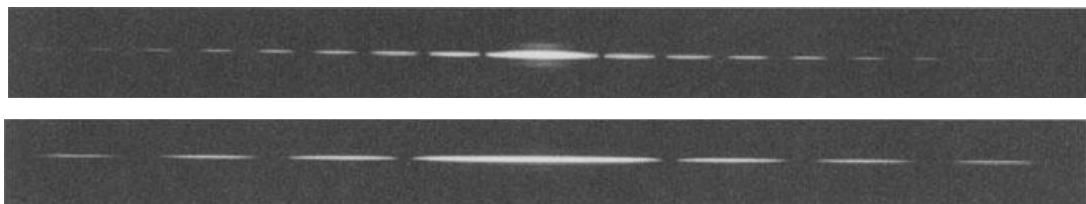


Fig. 9.9. Two experimentally obtained spectra of a long adjustable slit. The slit width a is smaller in the lower spectrum.

It is easy to see that a modulation will also appear in the v_y -direction, when the slit is of finite extent in the y -direction. To illustrate this case, Fig. 9.10 shows the diffraction pattern of a square aperture, obtained by illumination with a He–Ne laser. The modulation of the intensity in the v_x - and v_y -directions is obvious.

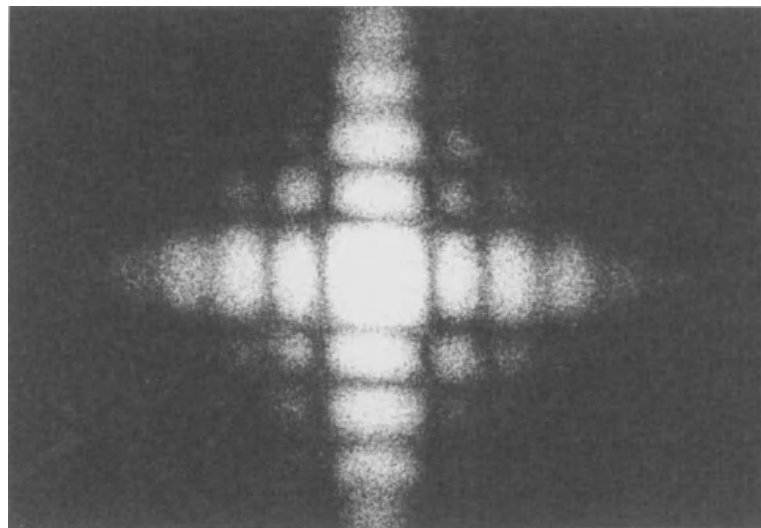


Fig. 9.10. Experimental diffraction pattern of a square aperture.

9.3.4 Two Point Sources

In Sect. 4.2 we considered the superposition of monofrequency spherical waves coming from two point sources. The far-field diffraction pattern given there can be calculated elegantly and simply with the formalism of the Fourier transform.

Let the two point sources be located on the x -axis, symmetrically to the origin, and have a separation of $2x_0$ (Fig. 9.11). This source arrangement leads to the electric field

$$E(x,y) = E_0 \delta(y) [\delta(x - x_0) + \delta(x + x_0)]. \quad (9.42)$$

The two-dimensional δ functions again are written as a product of one-dimensional δ functions. Then the far-field amplitude spectrum is given, along with (9.32), by

$$\mathcal{F}[E(x,y)] = \exp(-2\pi i v_x x_0) + \exp(2\pi i v_x x_0) = 2 \cos(2\pi v_x x_0). \quad (9.43)$$

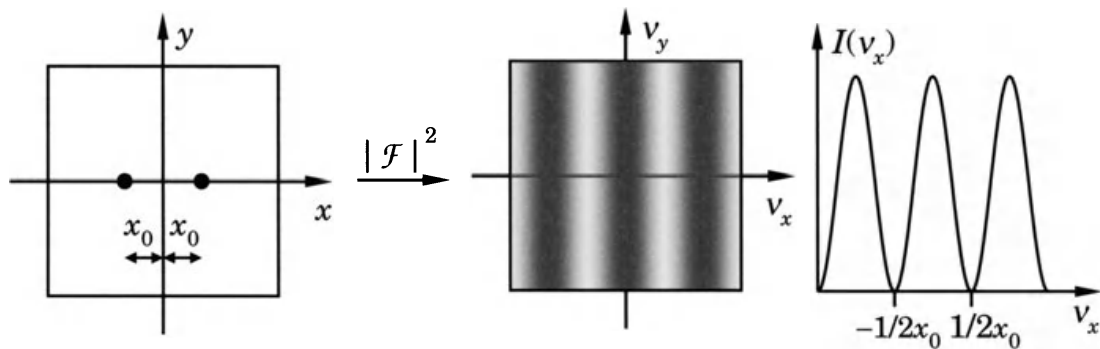


Fig. 9.11. Two point sources and their power spectrum.

The amplitude spectrum has a cosine modulation in the ν_x -direction with a spatial period of $1/x_0$, in the ν_y -direction the amplitude is constant. The intensity of the amplitude spectrum, the power spectrum of the input field, corresponds to a cosine grating:

$$|\mathcal{F}[E]|^2 = 4 \cos^2(2\pi \nu_x x_0) = 2(1 + \cos 4\pi \nu_x x_0). \quad (9.44)$$

Its fringe spacing is $\Delta\nu_x = 1/2x_0$, half the period of the amplitude spectrum.

9.3.5 Cosine Grating

In the previous example, we obtained a cosine grating as the intensity distribution in the Fourier spectrum of two point sources. This spectrum can be recorded on a photographic plate and used as the input pattern in a $2f$ arrangement. If we transilluminate the cosine grating with a plane wave and optically Fourier transform it, do we get the two point sources back?

The cosine grating, having the grating constant d , can be described by the transmittance (Fig. 9.12)

$$\begin{aligned} \tau(x,y) &= \cos^2\left(\pi \frac{x}{d}\right) = \frac{1}{2} + \frac{1}{2} \cos\left(\frac{2\pi x}{d}\right) \\ &= \frac{1}{2} + \frac{1}{4} \exp\left(i \frac{2\pi x}{d}\right) + \frac{1}{4} \exp\left(-i \frac{2\pi x}{d}\right). \end{aligned} \quad (9.45)$$

When it is illuminated with a plane monofrequency wave, the electric field is modulated accordingly:

$$E(x,y) = E_0 \tau(x,y) = E_0 \left[\frac{1}{2} + \frac{1}{4} \exp\left(i \frac{2\pi x}{d}\right) + \frac{1}{4} \exp\left(-i \frac{2\pi x}{d}\right) \right]. \quad (9.46)$$

The spectrum is easily obtained when we have knowledge of the Fourier transform of plane waves [see (9.34) and (9.36)]:

$$\begin{aligned} \mathcal{F}[E(x,y)] &= \frac{1}{2} E_0 \delta(\nu_y) \delta(\nu_x) && \text{0th order,} \\ &+ \frac{1}{4} E_0 \delta(\nu_y) \delta(\nu_x - 1/d) && \text{1st order,} \\ &+ \frac{1}{4} E_0 \delta(\nu_y) \delta(\nu_x + 1/d) && \text{-1st order.} \end{aligned} \quad (9.47)$$

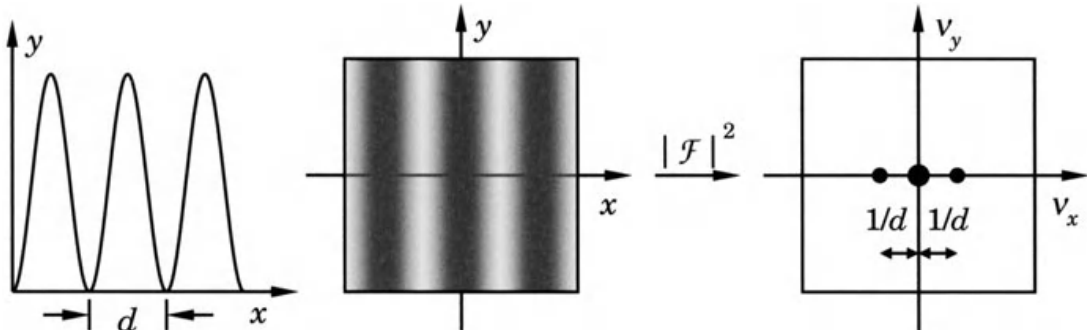


Fig. 9.12. Cosine grating and its power spectrum.

In the Fourier plane the spectrum is given by three points along the v_x -axis which have a separation of $1/d$, the inverse of the grating constant. The central point at the origin, the zeroth order, has twice the amplitude of the two other points (Fig. 9.12).

The spectrum of two points yields a cosine grating, the spectrum of a cosine grating, however, yields three points. Why? The reason is the intensity formation in between, which destroys the phase information. A negative transmittance is not possible with a passive grating. Therefore, the cosine grating transmittance must have a direct part (a nonzero average). This part leads to undiffracted light, a plane wave along the optical axis that in the spectrum gives rise to a point at the origin.

We came across a similar phenomenon when discussing stellar speckle interferometry. There, the averaged autocorrelation function of a stellar speckle pattern is calculated corresponding to the Fourier transform of the spatial power spectrum of the (disturbed) object. In this case, too, no phase information of the object wave is available. This leads to ambiguities and artifacts upon image reconstruction. The same problem is encountered when processing specklegrams in flow diagnostics, for instance. It is known as the ‘phase retrieval problem’.

9.3.6 Circular Aperture

A circular aperture of radius a is given by the transmittance

$$\tau(x, y) = \begin{cases} 1 & \text{for } x^2 + y^2 \leq a^2, \\ 0 & \text{otherwise,} \end{cases} \quad (9.48)$$

or, in polar coordinates (r, Θ) , connected with the Cartesian coordinates by the transformation $x = r \cos \Theta$, $y = r \sin \Theta$, by

$$\tau(r, \Theta) = \tau(r) = \begin{cases} 1 & \text{for } r \leq a, \\ 0 & \text{otherwise.} \end{cases} \quad (9.49)$$

Thus, for the light field behind the aperture,

$$E(r, \theta) = \tau(r)E_0, \quad (9.50)$$

we obtain the Fourier transform:

$$\mathcal{F}[E](v_x, v_y) = E_0 \int_0^{2\pi} d\Theta \int_0^a \exp[-2\pi i(r \cos \Theta v_x + r \sin \Theta v_y)] r dr. \quad (9.51)$$

Because of the rotational symmetry it is convenient also to transform the spectral coordinates (v_x, v_y) to polar coordinates. With the transformation $v_x = v \cos \varphi$, $v_y = v \sin \varphi$ we get:

$$\mathcal{F}[E] = E_0 \int_0^a r dr \int_0^{2\pi} \exp[-2\pi i v r \cos(\Theta - \varphi)] d\Theta. \quad (9.52)$$

Here, the relation $\cos(\Theta - \varphi) = \cos \Theta \cos \varphi + \sin \Theta \sin \varphi$ has been used. The substitution $\xi = \Theta - \varphi$ leads to an integral over the Bessel function J_0 defined by

$$J_0(s) = \frac{1}{2\pi} \int_0^{2\pi} \exp(is \cos \xi) d\xi = \frac{1}{2\pi} \int_0^{2\pi} \exp(is \sin \xi) d\xi. \quad (9.53)$$

In a first step, we obtain:

$$\mathcal{F}[E](v, \varphi) = 2\pi E_0 \int_0^a r J_0(-2\pi v r) dr. \quad (9.54)$$

The Bessel function J_0 is symmetric, that is, $J_0(-s) = J_0(s)$, and is connected with the Bessel function J_1 by

$$J_1(w) = \frac{1}{w} \int_0^w s J_0(s) ds. \quad (9.55)$$

Thus, we finally obtain the following for the amplitude spectrum of a circular aperture of radius a :

$$\mathcal{F}[E](v, \varphi) = \frac{E_0 a}{v} J_1(2\pi v a). \quad (9.56)$$

In Cartesian coordinates (v_x, v_y) this expression reads:

$$\mathcal{F}[E](v_x, v_y) = \frac{E_0 a}{\sqrt{v_x^2 + v_y^2}} J_1\left(2\pi a \sqrt{v_x^2 + v_y^2}\right). \quad (9.57)$$

The corresponding intensity distribution is given in Fig. 9.13. The central bright spot is called the Airy disk..

The first root in the radial direction occurs at

$$v_1 = \left(\sqrt{v_x^2 + v_y^2} \right)_1 = \frac{1.22}{2a}. \quad (9.58)$$

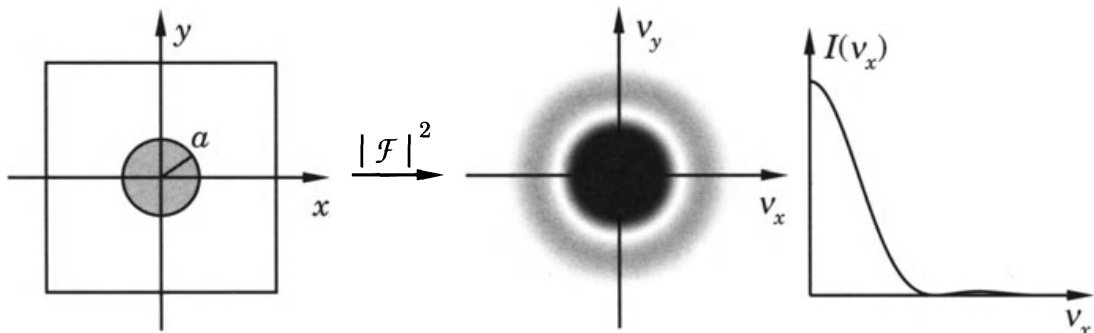


Fig. 9.13. Circular aperture and its power spectrum.

In optical instruments, circular apertures are usually applied as stops along the light path. Therefore, the Airy disk is often encountered in diffraction-limited imaging, for instance in microscopes or telescopes. The resolving power of these instruments is defined via the diameter of the Airy disk (see, for instance, [9.1]). Figure 9.14 shows two Airy disks and the adjacent diffraction rings obtained experimentally with two differently sized circular apertures. The actual intensity relation between the diffraction rings cannot be reproduced on paper because of the lack of grey scale dynamics.

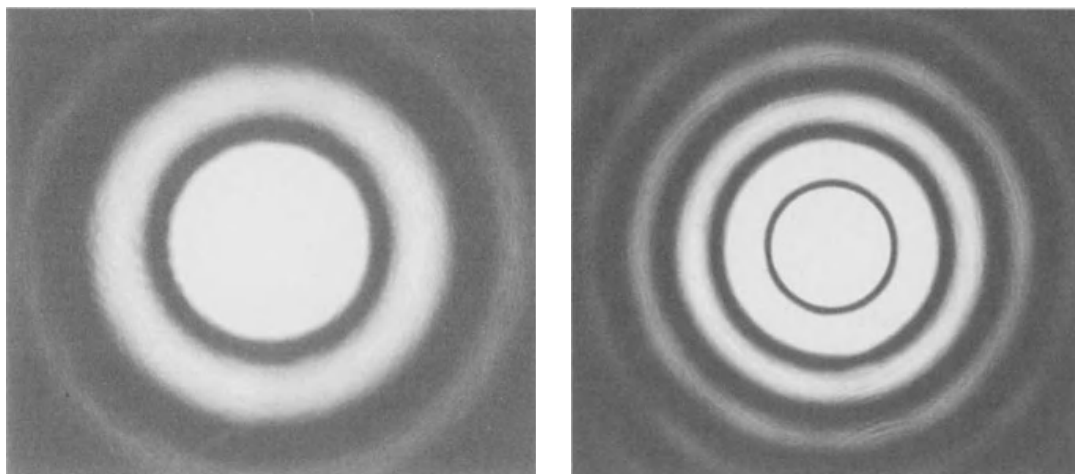


Fig. 9.14. The diffraction patterns of circular apertures of different radii.

9.3.7 Compound Diffracting Systems

In the examples considered so far, we observe recurrent relations between a diffracting pattern and its spectrum. For instance, a coarse structure as an input (a broad slit) yields a fine structure in the diffraction pattern (small distance between the maxima of the slit function). This is due to general relations valid for the Fourier transform.

In physics, the mathematical rules of the Fourier transform can be nicely illustrated optically.

The *linearity* of the Fourier transform,

$$\begin{aligned} \mathcal{F}[E_1(x,y) + E_2(x,y)](\nu_x, \nu_y) &= \mathcal{F}[E_1(x,y)](\nu_x, \nu_y) \\ &\quad + \mathcal{F}[E_2(x,y)](\nu_x, \nu_y), \end{aligned} \tag{9.59}$$

translates the superposition principle for light waves to the amplitude spectrum; that is, the Fourier transform of the superposition of two electric fields equals the superposition of the Fourier transform of the individual fields.

The *shift property* of the Fourier transform,

$$\begin{aligned}\mathcal{F}[E(x + \Delta x, y + \Delta y)](\nu_x, \nu_y) &= \exp[2\pi i(\nu_x \Delta x + \nu_y \Delta y)] \\ &\cdot \mathcal{F}[E(x, y)](\nu_x, \nu_y),\end{aligned}\quad (9.60)$$

states that only a linear phase shift is introduced when the diffracting pattern is shifted in x - and y -direction by Δx and Δy , respectively. The usual diffraction pattern, that is, the intensity of the amplitude spectrum, is not altered.

The *similarity property* of the Fourier transform,

$$\mathcal{F}[E(ax, by)](\nu_x, \nu_y) = \frac{1}{|a| \cdot |b|} \mathcal{F}[E(x, y)]\left(\frac{\nu_x}{a}, \frac{\nu_y}{b}\right), \quad (9.61)$$

corresponds to the fact that an enlargement of the diffracting pattern (for instance, by the broadening of a slit) leads to a corresponding reduction in size of the diffraction pattern. Similarly, the diffraction pattern gets larger upon reduction of the diffracting structure. As light cannot get lost in this transformation, the brightness of the diffraction pattern changes according to its size.

The *convolution relations* of the Fourier transform are especially helpful for understanding the Fourier spectra of compound diffracting objects. When the electric field $E(x, y)$ can be written as a product, $E(x, y) = E_1(x, y)E_2(x, y)$, then its amplitude spectrum is given as a convolution of the Fourier transform of the individual fields:

$$\mathcal{F}[E_1(x, y) \cdot E_2(x, y)](\nu_x, \nu_y) = \mathcal{F}[E_1(x, y)] * \mathcal{F}[E_2(x, y)]. \quad (9.62)$$

If, on the other hand, the input field can be written as a convolution of two fields,

$$E(x, y) = (E_1 * E_2)(x, y) = \int_{-\infty}^{+\infty} \int_{-\infty}^{+\infty} E_1(\xi, \eta) E_2(x - \xi, y - \eta) d\xi d\eta, \quad (9.63)$$

the amplitude in the far-field diffraction pattern is given by the product of the individual Fourier transforms:

$$\mathcal{F}[(E_1 * E_2)(x, y)](\nu_x, \nu_y) = \mathcal{F}[E_1(x, y)](\nu_x, \nu_y) \cdot \mathcal{F}[E_2(x, y)](\nu_x, \nu_y). \quad (9.64)$$

With these relations in mind, we can calculate the diffraction pattern of a grating consisting of M slits of width a and grating distance d ($> a$) in the x -direction (Fig. 9.15). The electric field behind the grating, when it is illuminated with a plane monofrequency wave at normal incidence, can be written as

$$E(x, y) = E_0 \sum_{m=1}^M \text{rect}\left(\frac{x}{a} - \frac{md}{a}\right) = E_0 \left[\sum_{m=1}^M \delta(x - md) \right] * \text{rect}\left(\frac{x}{a}\right). \quad (9.65)$$

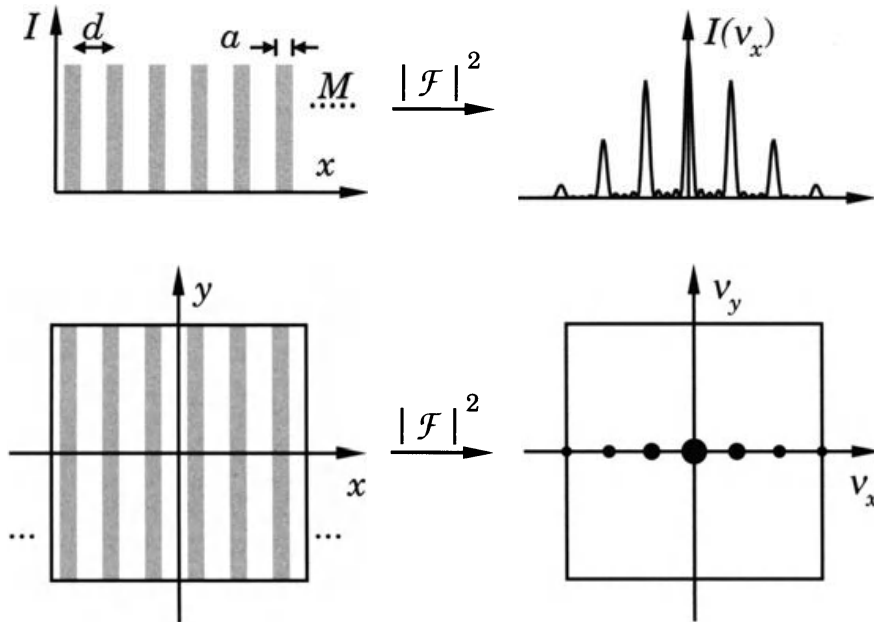


Fig. 9.15. Grating composed of m slits and its power spectrum.

Using linearity, the convolution relation, and the shifting property we get:

$$\begin{aligned} \mathcal{F}[E] &= E_0 \delta(\nu_y) \frac{\sin(\pi a \nu_x)}{\pi \nu_x} \sum_{m=1}^M \exp(-2\pi i m d \nu_x) \\ &= E_0 \delta(\nu_y) a \operatorname{sinc}(a \nu_x) \exp[-\pi i d \nu_x (M+1)] \frac{\sin(\pi M d \nu_x)}{\sin(\pi d \nu_x)}. \end{aligned} \quad (9.66)$$

When the intensity is calculated, the phase factor $\exp[-\pi i d \nu_x (M+1)]$ drops out:

$$I(\nu_x, \nu_y) = |E_0|^2 \delta(\nu_y) a^2 \operatorname{sinc}^2(a \nu_x) \frac{\sin^2(\pi M d \nu_x)}{\sin^2(\pi d \nu_x)}. \quad (9.67)$$

Looking at the diffraction pattern of this grating (see Fig. 9.15), we may discern the influence of the different components of the object. The coarse structure, proportional to $a^2 \operatorname{sinc}^2(a \nu_x)$, is determined by the individual slit, since the corresponding slit function forms the envelope of the diffraction pattern. The periodic repetition, on the other hand, becomes visible in a more detailed, periodic structuring of the spectrum [proportional to $\sin^2(\pi M d \nu_x)/\sin^2(\pi d \nu_x)$]. Thereby, the fine structure is determined by the grating size Md .

As an example for the spectrum of a compound diffracting system, Fig. 9.16 shows a honeycomb mesh and its spectrum. The hexagonal basic pattern being periodic, the spectrum is composed of a set of points showing the corresponding symmetries.

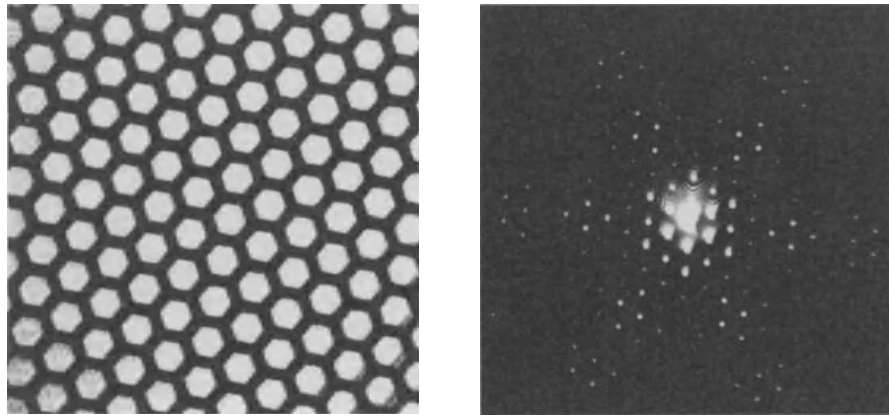


Fig. 9.16. Honeycomb mesh and its diffraction pattern.

9.4 Coherent Optical Filtering

As with the filtering of a time signal by the manipulation of its spectrum, a two-dimensional spatial pattern can be filtered by manipulating the optical spectrum in the spectral plane. Filter operations are employed for image enhancement, phase visualization and pattern recognition. For visualization of the filtered image, the modified spectrum has to be suitably transformed. The operation most suited would be the inverse Fourier transform. It cannot be realized by diffraction, however. But the Fourier transform, as given by a lens, yields the same result as we will see soon. This leads to the $4f$ arrangement, as it is called (Fig. 9.17).

The spectrum $F(u,v) = \mathcal{F}[f(x,y)]$ of the input pattern $f(x,y)$ is generated in the Fourier plane by lens 1. There, the spectrum may be modified, for instance, by letting only selected spatial frequency components pass. Thereby a field $F'(u,v)$ is generated. Lens 2 then produces a different image of the input pattern in the (\bar{x},\bar{y}) -plane: $f'(\bar{x},\bar{y}) = \mathcal{F}[F'(u,v)]$. Without filtering, the input pattern is retained; but it is upside down. This can

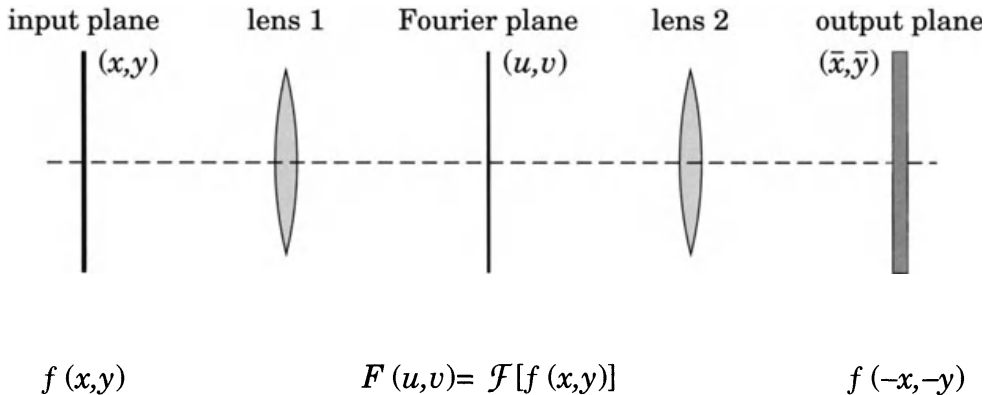


Fig. 9.17. The $4f$ arrangement.

be checked by following the imaging rays through the lens system or by applying the Fourier transform twice:

$$\mathcal{F}[\mathcal{F}[f(x,y)]] = f(-x, -y). \quad (9.68)$$

As with the filtering of one-dimensional signals, for instance, of electrical oscillations, the simplest way of manipulating the spectrum consists in rejecting certain frequency regions. This is done in the optical low-pass or high-pass filter.

9.4.1 Low-Pass Filter or Spatial Frequency Filter

Every optical system, because of its limited apertures, is an example of a low-pass filter: high spatial frequencies cannot pass. The extreme case is given by a pinhole with its idealized aperture function:

$$\tau(x,y) = \begin{cases} 1 & \text{for } (x,y) = (0,0), \\ 0 & \text{otherwise.} \end{cases} \quad (9.69)$$

Figure 9.18 shows a practical application: the spatial frequency filter, often simply called the spatial filter, we came across in holography. The incident laser beam is focused by a microscope objective at the pinhole. Then, in the focal plane (Fourier plane), we have the filtered amplitude spectrum

$$F'(\nu_x, \nu_y) = E_0 \delta(\nu_x, \nu_y) \quad \text{or} \quad F'(u, v) = E_0 \delta(u, v). \quad (9.70)$$

The zeroth diffraction order only can pass. The second lens transforms the point source into a plane wave ($\mathcal{F}[\delta] = 1$), independently of the field in the input plane. Those spatial frequencies that may be generated by diffraction at dust spots on lenses are filtered out. Thus any disturbances of the wave front are removed.

The second lens (collimating lens) simultaneously acts for beam expansion. The beam diameter grows proportionally to the focal length of the collimating lens.

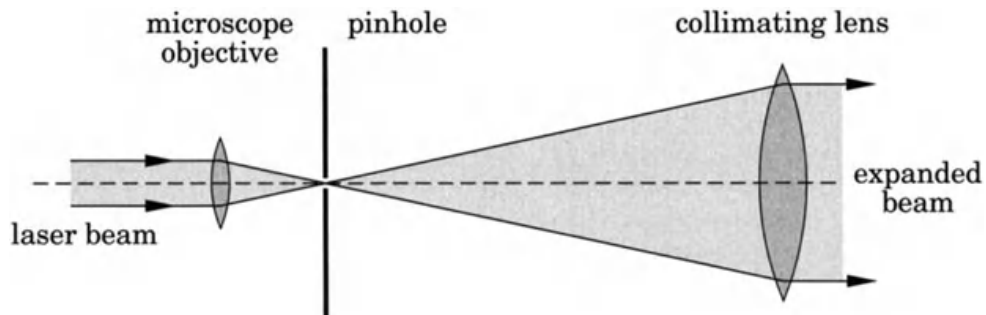


Fig. 9.18. Spatial frequency filter with a pinhole in the back focal plane of a microscope objective and a collimating lens. This unit acts as a beam expander with a homogeneous beam as output.

9.4.2 High-Pass Filter or Dark Field Method

With this filter, for rejecting all frequencies below a cutoff frequency, a disk is placed in the spectral plane. This way, edges are enhanced. By the loss of the ‘dc part’, however, the image usually becomes very dark. This type of filter is used in microscopy where it is called the dark field method. Practically little more than the zeroth order is rejected.

To begin, the effect of high-pass filtering is demonstrated with an amplitude object, the cosine grating discussed previously. The field of the grating in the object plane, along with (9.46) and $E_0 = 1$, can be written as

$$E(x,y) = \cos^2\left(\pi \frac{x}{d}\right) = \frac{1}{2} + \frac{1}{2} \cos\left(2\pi \frac{x}{d}\right). \quad (9.71)$$

In the spectral plane we have the field (see (9.47)):

$$\mathcal{F}[E(x,y)] = \delta(\nu_y) \left[\frac{1}{2} \delta(\nu_x) + \frac{1}{4} \delta\left(\nu_x - \frac{1}{d}\right) + \frac{1}{4} \delta\left(\nu_x + \frac{1}{d}\right) \right]. \quad (9.72)$$

When, as shown in Fig. 9.19, the zeroth order is eliminated from the spectrum by the high-pass filter, we have the modified spectrum:

$$\mathcal{F}_{hp}[E] = \delta(\nu_y) \frac{1}{4} \left[\delta\left(\nu_x - \frac{1}{d}\right) + \delta\left(\nu_x + \frac{1}{d}\right) \right]. \quad (9.73)$$

A second Fourier transform yields the field of the filtered image. We encountered this Fourier transform earlier when calculating the spectrum of two point sources [see (9.43)], so we are able to write down the result immediately. With $x_0 = 1/d$, we have:

$$\mathcal{F}[\mathcal{F}_{hp}[E]] = \frac{1}{4} 2 \cos\left(2\pi \frac{x}{d}\right) = \frac{1}{2} \cos\left(\pi \frac{x}{d/2}\right). \quad (9.74)$$

Notice that, after filtering, the image of the object has a structure twice as fine as it had originally, a substantial alteration (Fig. 9.19). The example shows that filter operations may have quite unexpected results.

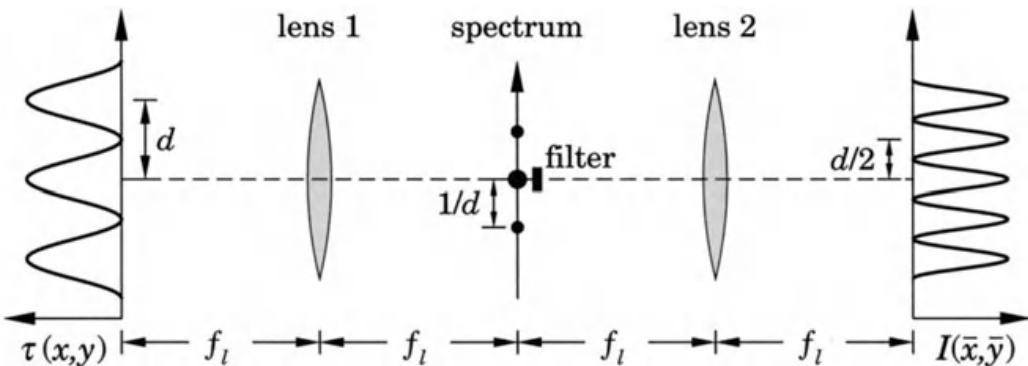


Fig. 9.19. Filtering a cosine grating with a high-pass filter.

The dark field method is most often used to visualize thin phase objects, for instance, thin sheets of organic specimens, air flows around bodies, vortices and shock waves in fluid flows, finger prints, strains in transparent materials, density alterations in heating, etc. In all these cases, only a spatial phase pattern is generated across the light beam, which has its origin in a spatially varying index of refraction. Without filtering, these phase patterns stay invisible, since phase modifications do not show up when forming the intensity. The field of a phase object is given by

$$E(x,y) \propto \tau(x,y) = a \exp[i\varphi(x,y)] \quad (a = \text{const}). \quad (9.75)$$

It is the phase pattern $\varphi(x,y)$ that contains the information on the object. The intensity of the field everywhere is the same:

$$I(x,y) = E(x,y)E^*(x,y) \propto \tau(x,y)\tau^*(x,y) = |a|^2 = \text{const}. \quad (9.76)$$

For thin phase objects, $|\varphi| \ll 2\pi$, the exponential function can be expanded to yield approximately:

$$\tau(x,y) \approx a[1 + i\varphi(x,y)]. \quad (9.77)$$

For simplicity, and since it does not alter the result, we assume that the phase distribution $\varphi(x,y)$ has zero mean. Due to the linearity of the Fourier transform we have

$$\mathcal{F}[\tau] = a(\delta(v_x)\delta(v_y) + i\mathcal{F}[\varphi(x,y)]). \quad (9.78)$$

Rejecting the zeroth order yields the high-pass filtered spectrum:

$$\mathcal{F}_{hp}[E] = ia\mathcal{F}[\varphi(x,y)]. \quad (9.79)$$

It no longer contains a dc term. The filtered image is formed by a further Fourier transform:

$$\mathcal{F}[\mathcal{F}_{hp}[E]] = ia\mathcal{F}[\mathcal{F}[\varphi(x,y)]] = ia\varphi(-x,-y). \quad (9.80)$$

Now, the intensity is no longer uniform, but makes visible the phase pattern φ :

$$I = |\mathcal{F}[\mathcal{F}_{hp}[E]]|^2 = a^2\varphi^2(-x,-y). \quad (9.81)$$

The intensity quadratically depends on the phase variation. For a constant phase the intensity vanishes. Therefore the visualized phase is given as a bright image on a dark background, thence the name dark field method.

9.4.3 Phase Filter or Phase Contrast Method

Up to now, we have considered amplitude filters only; that is, filters that stop some part of the spectrum and let the other pass. Pure phase objects

can be made visible with filters that influence the phase of a suitable part of the spectrum. For thin phase objects we wrote in the previous section:

$$\tau(x,y) = a(1 + i\varphi(x,y)). \quad (9.82)$$

In this approximation we have a real dc term and a purely imaginary phase term. Because of the linearity of the Fourier transform, the dc term is shifted in phase by $\pi/2$ relative to the remaining part of the Fourier spectrum:

$$\mathcal{F}[\tau] = a(\delta(\nu_x)\delta(\nu_y) + i\mathcal{F}[\varphi(x,y)]). \quad (9.83)$$

If the zeroth order were shifted in phase by $\pi/2$, we would get an amplitude modulation in the image that is visible, in contrast to a pure phase modulation. A filter having this property can be fabricated quite easily. One only has to insert a quarter wave plate into the zeroth order. It shifts the phase of the field in the origin of the spatial frequency plane by $\pi/2$. Then, in (9.83) the dc term is multiplied by $\exp(i\pi/2) = i$, and the phase filtered spectrum is obtained:

$$\mathcal{F}_{\text{pf}}[\tau] = ai(\delta(\nu_x)\delta(\nu_y) + \mathcal{F}[\varphi(x,y)]). \quad (9.84)$$

A further Fourier transform yields the filtered image:

$$\mathcal{F}[\mathcal{F}_{\text{pf}}[\tau]] = ai(1 + \varphi(-x, -y)). \quad (9.85)$$

Now, the intensity reads:

$$\begin{aligned} I_{\text{pf}} &= a^2 [1 + 2\varphi(-x, -y) + \varphi^2(-x, -y)] \\ &\approx a^2 (1 + 2\varphi(-x, -y)). \end{aligned} \quad (9.86)$$

In the last line, the term φ^2 is omitted, since we have assumed a weak phase modulation ($|\varphi| \ll 2\pi$).

Compared to the dark field method, now a linear relationship between image intensity and phase φ is obtained. This leads to an increased sensitivity for weak phase objects. The method is called the phase contrast method and was developed by *Frits Zernike* (1888–1966).

The method can be improved in a number of ways. The contrast in the image, for instance, is lowered by the dc term a^2 . Therefore, the phase contrast method is combined with an attenuation of the amplitude of the zeroth order by a factor b ($0 < b < 1$):

$$I_{\text{pf}} = a^2 [b^2 + 2b\varphi(-x, -y)]. \quad (9.87)$$

Thus, although the intensity of the image decreases, the contrast is nevertheless increased.

9.4.4 Half-Plane Filter or Schlieren Method

The schlieren method also may be used to make phase objects visible [9.2]. In this case, again an amplitude filter is employed. One half of the spatial frequency plane is rejected (for instance, with a knife edge), including half of the zeroth order. This has the effect that in the filtered image the intensity is approximately proportional to the gradient of the phase (dependent on the orientation of the half plane):

$$I(-x, -y) \propto \left| \frac{\partial \varphi(x, y)}{\partial x} \right|. \quad (9.88)$$

This method achieves its task by disturbing the balance of the spectral components which leads to a uniform intensity of the image.

9.4.5 Raster Elimination

When an image is printed, it is difficult to generate shades of grey. Therefore, the image is sampled and the halftones are generated by inserting differently sized dots at the sample points. The same problem appears in digital image processing. The image must be sampled in the x -, the y - and even the z -direction and stored as a matrix of pixels (picture elements, two-dimensional) or voxels (volume picture elements, three-dimensional). How do we perceive grey scales in these images?

The sampling theorem we briefly mentioned in connection with digital holograms relates the sampled and the original image. It states that the original image can be restored exactly from the sampled image when it is bandlimited, that is, when it contains spatial frequencies up to a cutoff frequency only, and when the distance between adjacent sample points is not larger than a certain value determined by the cutoff frequency.

Mathematically, a sampled image (look closely at any halftone picture of this book) can be formulated in the following way:

$$g_s(x, y) = \text{comb}\left(\frac{x}{a}\right) \text{comb}\left(\frac{y}{b}\right) g(x, y). \quad (9.89)$$

The comb function,

$$\text{comb}\left(\frac{x}{a}\right) = \sum_{-\infty}^{+\infty} \delta(x - na), \quad (9.90)$$

describes the sampling; the function $g(x, y)$ describes the continuous (complex) amplitude distribution of the original image. The pixel distances in the x - and the y -directions are a and b , respectively.

The spectrum of $g_s(x, y)$ is obtained from the spectrum of the continuous image, $G(v_x, v_y) = \mathcal{F}[g(x, y)](v_x, v_y)$, by means of the convolution relation

$$\mathcal{F}[g_s(x, y)] = G_s(v_x, v_y) = a \text{comb}(av_x) b \text{comb}(bv_y) * G(v_x, v_y). \quad (9.91)$$

Here, we have used the fact that the Fourier transform of a comb function again is a comb function.

Thus, the Fourier transform of the sampled image yields a grid that arises by repetition of the spectrum of the original image at each grid point. The vicinity of each grid point of the spectrum contains the complete information about the original image. Therefore, the grid points in the Fourier plane should have such a large distance that the individual, identical spectra do not overlap. When the vicinity of a single grid point in the spectrum of $g_s(x, y)$ is taken and the rest of the plane rejected, the original image is obtained by a Fourier transform. This type of filtering can be thought of as a multiplication of the spectrum $G_s(v_x, v_y)$ with an aperture function acting as a low-pass filter. A circular aperture of suitable diameter or a rectangular aperture of suitable size (edge lengths $1/a$ and $1/b$) may be taken as a low-pass filter. Mathematically formulated, we get

$$\mathcal{F}[G_{sf}(v_x, v_y)] = \mathcal{F}[G_s(v_x, v_y)A(v_x, v_y)] = g_s(-x, -y) * \mathcal{F}[A(v_x, v_y)], \quad (9.92)$$

This is the convolution of the sampled image with the Fourier transform of the aperture function $A(v_x, v_y)$.

9.4.6 Demonstration Experiment

An experimental arrangement for demonstrating the filtering operations discussed above is given in Fig. 9.20. The $4f$ geometry of Fig. 9.17 has been augmented by a few components to simultaneously project the original image, its power spectrum, the filtered power spectrum, and the filtered image. In particular, large beam splitters are inserted into the main path to image the different planes onto a screen. In this way, the result of different optical filters can immediately be visualized.

Figure 9.21 shows an example for the influence of low-pass filtering on a halftone image. The upper row presents the halftone image (left) and its spectrum (right). In the lower row, the filtered spectrum (right) and the corresponding filtered image (left) are to be seen. The original raster points have disappeared and a grey-scale picture is obtained. However, the printing process has added a new grid.

9.4.7 Holographic Filters

Up to now, we have filtered images in the Fourier plane by rejecting certain spatial frequency regions. With these filters, except for in the phase contrast method, only the amplitude of the light wave has been influenced. The most general filter, a filter with complex transmittance, would modulate the amplitude and phase of the spectral field distribution as a function of (v_x, v_y) or (u, v) . Filters of this kind are difficult to produce